

# Photoemission electron microscopy of exciton-polaritons in thin $\text{WSe}_2$ waveguides

Tobias Eul,<sup>\*,†</sup> Miwan Sabir,<sup>†</sup> Victor DeManuel-Gonzalez,<sup>†</sup> Florian Diekmann,<sup>†</sup> Kai Rosnagel,<sup>†,‡</sup> and Michael Bauer<sup>†,‡</sup>

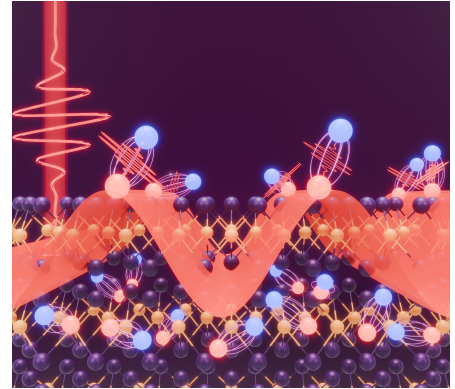
<sup>†</sup>*Institute of Experimental and Applied Physics, Kiel University, 24098 Kiel, Germany*

<sup>‡</sup>*Kiel Nano, Surface and Interface Science KiNSIS, Kiel University, 24118 Kiel, Germany*

E-mail: eul@physik.uni-kiel.de

## Abstract

Exciton-polaritons emerging from the interaction of photons and excitons in the strong coupling regime are intriguing quasiparticles for the potential exchange of energy during light-matter interaction processes such as light harvesting. The coupling causes an energy anti-crossing in the photon dispersion centered around the exciton resonance, i.e., a Rabi splitting between a lower and upper energetic branch. The size of this splitting correlates with the coupling strength between the exciton and the photonic modes. In this work, we investigate this coupling between excitons and photonic waveguide modes excited simultaneously in thin-film flakes of the transition-metal dichalcogenide  $\text{WSe}_2$ . Using a Photoemission electron microscope, we are able to extract the dispersion of the transversal electric and magnetic modes propagating through these flakes as well as extract the energy splitting. Ultimately, our findings precipitate the investigation of the propagation of exciton-polaritons in the time-domain via time-resolved photoemission.



## Introduction

Excitons, bound electron-hole pairs, are the focus of numerous experimental and theoretical research efforts based on their potential for light-driven energy harvesting. From the many semiconducting materials exhibiting excitonic resonances, transition-metal dichalcogenides (TMDC) have garnered special interest in recent years since they exhibit excitons with large

binding energies.<sup>1-4</sup> Embedding TMDC films or even monolayers within micrometer-sized cavities creates a suitable environment for a strong interaction between excitons and photons.<sup>5-10</sup> This interaction facilitates the formation of the light-matter quasiparticle termed exciton-polaritons.<sup>11,12</sup> Its hybrid nature promises new avenues for the energy exchange between light and matter and thus new technological developments.

The transfer of energy via the propagation of such a quasiparticle is especially interesting. Therefore, the interaction of excitons with propagating light modes rather than spatially confined cavity photons may provide another suitable environment for exciton-polaritons. Essentially, thin films of TMDC materials themselves host the necessary waveguiding modes, which are able to interact with the intrinsic exciton resonances.<sup>13</sup> Recent near-field studies involving scanning-near field microscopy (SNOM)<sup>14,15</sup> as well as cathode luminescence (CL)<sup>16</sup> focused on this particular approach for exciton-polaritons and discussed their spectroscopic signatures in thin films of WSe<sub>2</sub> and MoSe<sub>2</sub>. The dispersion of these polaritons exhibits a distinct energy anti-crossing centered around the exciton resonance, as illustrated in Fig. 1(a).

Photoemission electron microscopy (PEEM) is another experimental technique showcasing a significant sensitivity to the electric near-field as well as surface waves in metals<sup>17-26</sup> and photonic materials.<sup>27-33</sup> Furthermore, it is possible to measure dispersion relations of these propagating modes by tuning the wavelength of the exciting laser.<sup>27,34-36</sup> The direct imaging of the surface in PEEM in combination with pump-probe excitation schemes additionally facilitates tracing the propagation of waves and quasiparticles along the surface in the time domain.<sup>21,37-39</sup> This makes it a promising method for tracing the propagation of exciton-polaritons in real-time. Ultimately, time-resolved PEEM may even reveal highly local information on the energy transfer, i.e., the Rabi oscillation, between exciton and waveguide mode on an ultrafast timescale.

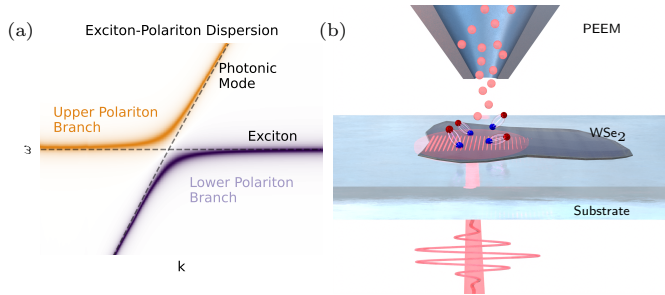


Figure 1: **Exciton-polariton dispersion and experimental scheme.** (a) Schematic illustration of the exciton-polariton dispersion. (b) Experimental setup with thin WSe<sub>2</sub> flakes situated on a transparent glass substrate. A laser illuminates the flake from the bottom, where it excites the exciton-polaritons as well as generates the photoelectrons, which enter the PEEM lens system.

## Results and Discussion

In this work, we demonstrate the capability of the PEEM technique to measure the dispersion relation of exciton-polaritons in thin WSe<sub>2</sub> films and determine the coupling strength between the A-exciton and photonic waveguide modes from this data. Fig. 1(b) depicts our experimental geometry. A laser with a tunable center wavelength in the range of 695 - 900 nm illuminates the TMDC sample from the bottom and a high electric field accelerates the photoelectrons carrying the information on the quasiparticle interactions into the PEEM column. Ref. <sup>40</sup> gives a more detailed description of this setup. We prepared the WSe<sub>2</sub> flakes on indium-tin-oxide (ITO) coated glass substrates via the mechanical exfoliation method. This method yields flakes with clean, flat surfaces and well defined edges albeit with varying thicknesses (20 - 150 nm) and lateral dimensions (5 - 50 μm). Prior to the PEEM experiments, we measured the thickness of the flakes with an atomic force microscope (AFM). Fig. 2(a) shows the AFM image for an exemplary WSe<sub>2</sub> flake, which exhibits a thickness of approximately 55 nm as well as sizes of 30 μm and 25 μm in x- and y-direction, respectively.

The corresponding PEEM image in Fig. 2(b), recorded with a mercury discharge lamp at a photon energy of  $E_{\text{ph}} = 4.9 \text{ eV}$ , shows the topography based on work function differences of the substrate and the WSe<sub>2</sub> flake. In order to reduce the work function of our samples

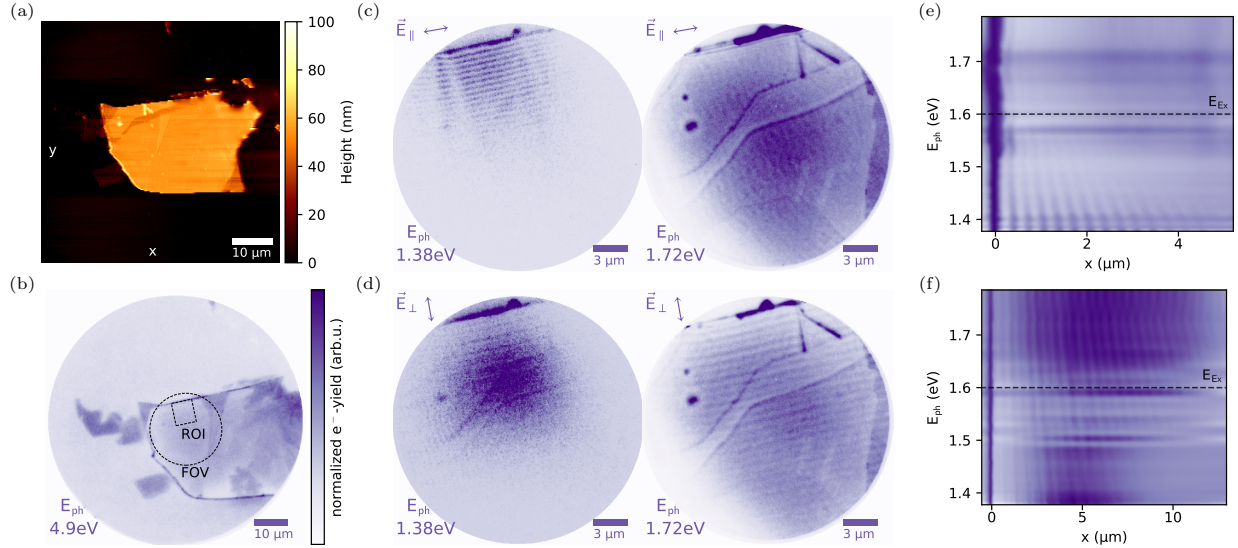


Figure 2: **Waveguide mode excitation in WSe<sub>2</sub> investigated using PEEM.** (a) AFM image of a WSe<sub>2</sub> flake with a thickness of approximately 55 nm. (b) PEEM image of the same flake recorded with a photon energy of 4.9 eV. The dashed circle (FOV) indicates the field of view of the detailed measurement in (c,d). The dashed square (ROI) indicates the region of interest for the extraction of the wave patterns. (c,d) PEEM images recorded with photon energies of 1.38 eV (left) and 1.72 eV (right) with the polarization parallel and perpendicular to the upper edge of the flake, respectively. (e,f) Extracted wave patterns for parallel and perpendicular polarization as a function of excitation photon energy, respectively. The dashed line indicates the energy  $E_{\text{Ex}}$  of the A-exciton of WSe<sub>2</sub>.

and as is customary for the PEEM-method,<sup>25,35,36,41,42</sup> we initially evaporated a fraction of a monolayer of an alkali metal (K) on the surface to reach the two-photon photoemission (2PPE) limit. In this limit, we are able to generate photoelectrons with the same laser pulses that excite the exciton-polaritons. The dashed circle (FOV) in Fig. 2(b) highlights the field of view, where we zoomed in on the sample to get close up images of the optical near-field of the waveguide modes. The dashed square (ROI) on the other hand marks the region of interest used for the subsequent quantitative analysis. For the experiment, we focus our laser onto the edge of the flake visible at the border of the ROI. Here, the light can couple into different waveguide modes, depending on the in-plane polarization with respect to this edge. The waveguide mode propagates through the flake and its electric field interferes with that of the second photon in the 2PPE-process resulting in a wave pattern in the photoemission contrast on the surface.<sup>20,43</sup> To investigate the dispersion relation of these modes, we excite the flake edge with varying photon energies around the exciton resonance and examine the photoemitted wave patterns.

Figs. 2(c,d) show exemplary images for the photon energies  $E_{\text{ph}} = 1.38 \text{ eV}$  and  $E_{\text{ph}} = 1.72 \text{ eV}$ , respectively, recorded with the polarization parallel (top) and perpendicular (bottom) to the edge. In the case of parallel polarization, we see a distinct wave pattern for the low photon energy, whereas just one single period of a wave is visible for the large photon energy. This result was to be expected based on the absorption properties of  $\text{WSe}_2$  above the energy  $E_{\text{Ex}} \approx 1.6 \text{ eV}$  of the A-exciton in  $\text{WSe}_2$ .<sup>14</sup> This absorption influence should be even more apparent in our experiment due to the nonlinear 2PPE excitation scheme. The wave patterns also clearly exhibit different periods hinting at the dispersion of the photonic mode. For perpendicular polarization on the other hand, the wave pattern remains observable for both photon energies. Figs. 2(e,f) illustrate this more clearly in a comparison of the wave patterns at all measured photon energies. For the data comparison, we sum up the intensity in the ROI of the PEEM image along the direction of the edge. As expected, the waves for parallel polarization in (e) show a decreasing propagation length with increasing photon energy. Surprisingly, in the case of perpendicular polarization in (f) the propagation length does not differ significantly over the measured spectral region. Since the exciton resonance is largely responsible for the absorption in this spectral region, it appears as if the waveguide mode excited via perpendicular polarization does not interact with the exciton, at least for this particular thickness of the flake.

The next step of the analysis is to directly extract the dispersion of the photonic modes from the wave patterns. By applying the Fast Fourier Transform (FFT) method to the wave patterns, we can analyze their periods in terms of the amplitude in Fourier space depending on the wavenumber  $k$  relative to the wavenumber  $k_0$  of light in free space. Since the wave patterns are not ideal signals with decay and constant offset, we apply a high-pass filter prior to the FFT, which removes low-frequency contributions from the signal. Fig. 3 shows the results of this method in dispersion plots consisting of the extracted Fourier signal after normalization to its respective maximum for each photon energy and subsequent interpolation. The normalization is necessary, since the experiment conditions such as focal spot size, intensity and, most importantly for the 2PPE process, the pulse durations vary for each individual photon energy. Images (a,c) show the experimental data obtained from the wave patterns in Figs. 2(e,f), respectively. The dispersion for the polarization parallel to the edge in (a) clearly shows one of the characteristic signatures of strong coupling between

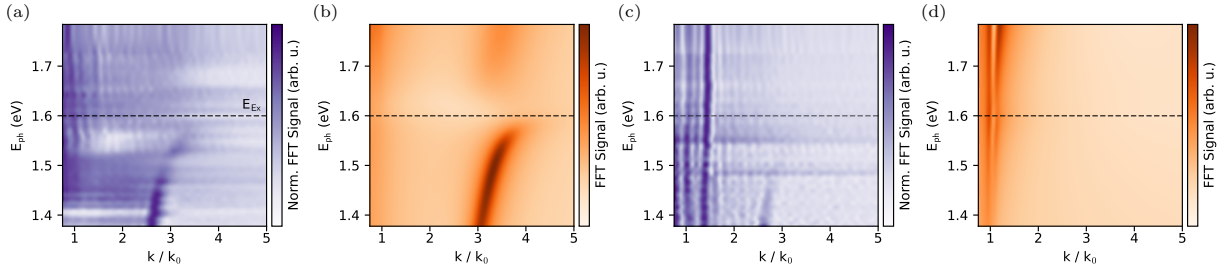


Figure 3: **Waveguide mode dispersion.** Dispersion curves extracted from the Fourier transformation of measured and simulated wave patterns. The wave numbers  $k$  are relative to the wave number of light in vacuum  $k_0$ . (a,c) Experimental data for polarization parallel and perpendicular to the excitation edge, respectively. (b,d) FDTD simulations for polarization parallel and perpendicular to the excitation edge, respectively. Simulated data for a flake thickness of 55 nm.

exciton and photonic mode, i.e., the lower polariton branch bending in the vicinity of the exciton resonance. The upper branch is not visible due to the strong absorption in this spectral region.

Examining the result for the perpendicular polarization  $E_{\perp}$  in (c), we first of all notice the same feature as in (a), albeit with a low intensity. This stems from the polarization not being perfectly perpendicular to the edge of the WSe<sub>2</sub> flake. More importantly, we see a linearly dispersing feature that does not show any deviation from its shape around the exciton resonance. This mode obviously does not interact with the exciton.

We additionally simulated the experiment by means of the finite-difference time-domain method<sup>44</sup> and using the optical constants for WSe<sub>2</sub> from Ref.<sup>45</sup> We use a broadband gaussian source, which covers the spectral range of the experimental data, and focus it on an edge of a thin film of WSe<sub>2</sub>. Equivalently, we extract the electric field wave patterns from a frequency monitor situated in the WSe<sub>2</sub> film and subsequently apply the FFT method. Here, we forego the normalization of the Fourier amplitude for each individual photon energy to retain the information about the absorption. Images (b,d) show the simulated dispersions corresponding to the experimental data in (a,c), i.e., a thickness of 55 nm and  $E_{\parallel}$ ,  $E_{\perp}$ , respectively. They reproduce the experiment reasonably well, albeit with a difference in the absolute values of  $k/k_0$ , which is probably due to differences in the optical constants for the simulations and the actual sample. For an excitation with  $E_{\parallel}$  in (b), the lower branch disperses similarly to the one obtained from the experiment. However, here we can additionally see the upper branch with a significantly reduced intensity and larger linewidth than the lower branch. When analyzing the individual electric field components, it becomes evident that the largest contribution to the total electric field, and therefore the dispersion signal, comes from the component parallel to the excitation edge. Since the waveguide mode propagates in the direction perpendicular to the edge, we can attribute the dispersive feature to a transversal electric (TE) mode.

Similarly, we determine from the simulation data in (d) that the light with  $E_{\perp}$  couples into a transversal magnetic (TM) mode. The dispersion in this case appears to be linear without any sign of interaction with the exciton. The experimental data and simulation in

(c) and (d) also exhibits another feature at  $k/k_0 = 1$ , i.e., a mode that follows the light line in free space from the excitation source. To summarize, the data show that for this particular thickness of the WSe<sub>2</sub> flake, we are able to control the exciton-photon coupling with the laser polarization being the experimental control parameter. We can either couple into the TE-mode for strong coupling or into the TM-mode for a freely propagating waveguide mode. However, additional own simulations (not shown) and similar results in<sup>14</sup> show that for increasing flake thickness  $\gtrsim 70$  nm the exciton also starts to couple to the TM-mode.

Ultimately, we are interested in the coupling strength of the exciton-polariton, which can be determined from the energy splitting in the dispersion curve. For this, we examine another WSe<sub>2</sub> flake with a significantly smaller thickness so that the absorption is overall reduced. As mentioned above, in this thickness range only the TE-mode couples to the exciton. Fig. 4(a) shows the PEEM image for this flake recorded at  $E_{\text{ph}} = 1.55$  eV with the polarization of the laser oriented parallel to the excitation edge at the bottom. The dashed square (ROI)

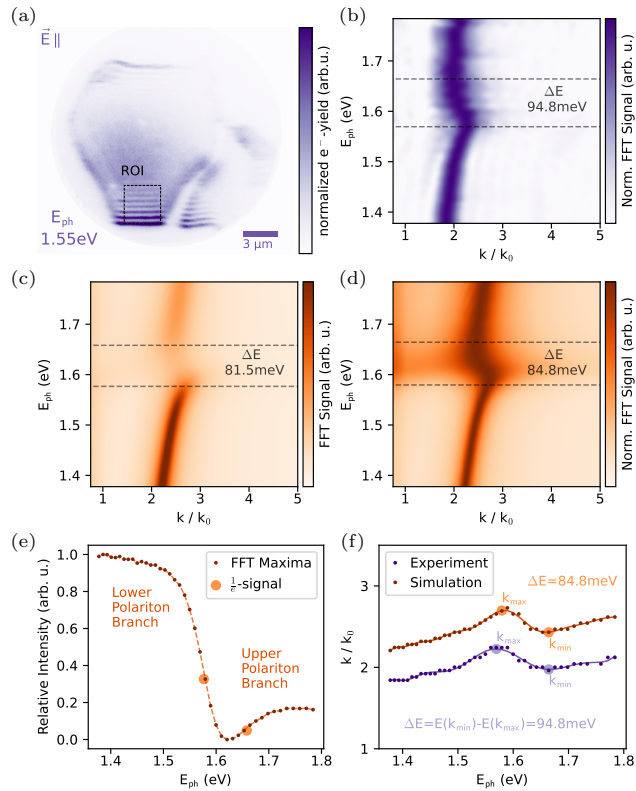


Figure 4: **Strong-coupling energy splitting.** (a) PEEM image of a WSe<sub>2</sub> flake recorded with a photon energy of 1.55 eV and laser polarization oriented parallel to the bottom edge. The dashed square (ROI) indicates the region of interest for the extraction of the wave patterns. (b) Dispersion of the TE-mode evaluated from the experimental data. (c,d) Simulated dispersion for a thickness of 30 nm without and with normalizing the signal of each individual frequency. (e) Extracted maximum FFT signals from (c) for determining the energy splitting based on exponential reduction of the branch intensities. (f) Extracted maxima positions from (b) and (d) for determining the energy gaps based on turning points in the dispersion.

marks the region of interest for the analysis of the wave patterns. Since the absorption is now reduced, we can resolve both the lower and the upper branch of the exciton-polariton in the dispersion curve in Fig. 4(b). Due to the individual normalization of the signal for each photon energy, we do not see a gap around the exciton resonance. Nevertheless, we can assign an energy splitting between the two branches based on the turning points within the two polariton branches. This becomes more evident when analyzing the corresponding FDTD simulations for a thickness of 30 nm in Figs. 4(c,d).

The two simulated dispersion plots show the same dispersion data without normalization in (c) and with normalization of the signal for each photon energy equivalent to the experimental data in (d). From the data without normalization, it is possible to extract the energy splitting in a straightforward manner by analyzing the intensity distribution of the two branches. Fig. 4(e) shows the relative maximum intensity of the branches extracted for each photon energy. In both branches we determine the point where the intensity has decreased to the  $\frac{1}{e}$ -fraction. We take the energy difference between these two points as a measure for the energy splitting of the dispersion curve. For the examined flake thickness, the analysis yields an energy splitting of  $\Delta E = 81.5$  meV. The dashed lines in Fig. 4(c) mark the extracted limits and the splitting. For the normalized data, we evaluate the energy splitting based on the two turning points in the dispersion curve located between the two branches that are clearly visible in Fig. 4(d).

For the quantitative analysis, we extract the  $k/k_0$ -values of the maximum in the dispersion for each photon energy and approximate this  $k(E_{\text{ph}})$  relation by applying a Savitzky-Golay filter on the data points. Fig. 4(f) shows this relation in orange for the simulated data. The curve shows a clear local maximum and minimum, which we identify as the  $k/k_0$ -values of the turning points. The corresponding photon energies at these points yield a value for the energy splitting of  $\Delta E = 84.4$  meV. This value is very close to the one extracted from the unnormalized data, which validates this approach. We therefore apply the equivalent procedure to the experimentally determined dispersion curve. The data from this analysis, shown as a blue line in Fig. 4(f), yields an energy splitting of  $\Delta E = 94.8$  meV for the exciton-polariton.

This value is in good agreement with the results of a SNOM study on exciton-photon coupling in MoSe<sub>2</sub> flakes.<sup>15</sup> Conversely, the above mentioned CL study on WSe<sub>2</sub> flakes<sup>16</sup> discusses larger values of up to 300 meV. The latter is surprising at first, since the crystals used to produce the flakes came from the same source as in our study. However, the actual preparation method differed. We prepared our samples via mechanical exfoliation, in contrast to the liquid-phase method used for the CL work. The different results indicate that the coupling strength between exciton and waveguide mode can be influenced by the preparation process, e.g. by different interaction strengths between adjacent layers of the TMDC flakes. Additionally, the electron beams used in CL studies induce another photon source, namely the Cherenkov radiation, which may significantly increase the interaction strength with the excitons.<sup>46</sup>

## Conclusion

In summary, we studied and analyzed the coupling strength between photonic waveguide modes and the A-exciton in thin-film WSe<sub>2</sub> flakes. By varying the photon energy as well as the polarization of the exciting laser, we were able to extract the dispersion relation of different modes from the near-field wave patterns recorded with PEEM. Additional FDTD simulations reproduced the experimental dispersion curves and provided us another avenue to analyze the strong coupling and the associated energy splitting between the lower and upper polariton branch. The simulations affirmed the nature of the modes, i.e., TE or TM for a polarization parallel or perpendicular to the excitation edge, respectively. With our experiment, we ascertained the challenge in accessing the upper polariton branch using nonlinear photoemission due to a strong absorption in WSe<sub>2</sub> for this spectral region. Nevertheless, we were able to extract the energy splitting from the turning points in the normalized dispersion curve, with  $\Delta E$  in the order of 100 meV for the exciton-polariton formed from the TE-mode.

In comparison, PEEM provides similar information as the scanning near-field microscopy technique employed in previous work on exciton-polaritons.<sup>14,15</sup> For example, the extracted energy splitting compares well to the splitting of 100 meV observed with SNOM in thin films of MoSe<sub>2</sub>. While SNOM allows to perform experiment under ambient conditions, PEEM, in combination with varying the laser polarization, is more flexible in selectively exciting the different TE or TM modes. Additionally, the parallel imaging of the surface, in contrast to scanning over it, allows for a faster data acquisition, and therefore facilitates an easier combination with pump-probe techniques for ultrafast time-domain studies. We expect that time-resolved PEEM will provide a new avenue to investigate the propagation of exciton-polaritons as well as the periodic energy exchange between the involved quasiparticles in real time.

## Associated content

### Data Availability Statement

The data that support the findings of this study are openly available in Zenodo at <http://doi.org/10.5281/zenodo.14168816>.

## Author information

### Author contributions

M.B. conceived the ideas and designed the experiments. T.E. carried out the PEEM experiments, the FDTD simulations and is responsible for the data evaluation. F.D. and K.R. synthesized the WSe<sub>2</sub> crystals. M.S. performed the mechanical exfoliation of the WSe<sub>2</sub> flakes onto the ITO substrates. V.D.G. carried out the AFM measurements. T.E. and M.B. wrote the manuscript.



## Acknowledgements

The PEEM study and the sample growth was supported by the German Research Foundation (DFG) through Projects 499426961 and 434434223 (CRC 1461), respectively. The authors acknowledge Prof. Dr. Nahid Talebi for fruitful discussions regarding the comparison of the PEEM and CL data.

## References

- (1) Cheiwchanchamnangij, T.; Lambrecht, W. R. L. Quasiparticle band structure calculation of monolayer, bilayer, and bulk MoS<sub>2</sub>. *Phys. Rev. B* **2012**, *85*, 205302, DOI: 10.1103/PhysRevB.85.205302.
- (2) Chernikov, A.; Berkelbach, T. C.; Hill, H. M.; Rigosi, A.; Li, Y.; Aslan, B.; Reichman, D. R.; Hybertsen, M. S.; Heinz, T. F. Exciton Binding Energy and Nonhydrogenic Rydberg Series in Monolayer WS<sub>2</sub>. *Phys. Rev. Lett.* **2014**, *113*, 076802, DOI: 10.1103/PhysRevLett.113.076802.
- (3) Zhu, B.; Chen, X.; Cui, X. Exciton Binding Energy of Monolayer WS<sub>2</sub>. *Scientific Reports* **2015**, *5*, 9218, DOI: 10.1038/srep09218.
- (4) Wang, G.; Chernikov, A.; Glazov, M. M.; Heinz, T. F.; Marie, X.; Amand, T.; Urbaszek, B. Colloquium: Excitons in atomically thin transition metal dichalcogenides. *Rev. Mod. Phys.* **2018**, *90*, 021001, DOI: 10.1103/RevModPhys.90.021001.
- (5) Dufferwiel, S. et al. Exciton–polaritons in van der Waals heterostructures embedded in tunable microcavities. *Nature Communications* **2015**, *6*, 8579, DOI: 10.1038/ncomms9579.
- (6) Liu, X.; Galfsky, T.; Sun, Z.; Xia, F.; Lin, E.-c.; Lee, Y.-H.; Kéna-Cohen, S.; Menon, V. M. Strong light–matter coupling in two-dimensional atomic crystals. *Nature Photonics* **2015**, *9*, 30–34, DOI: 10.1038/nphoton.2014.304.
- (7) Lundt, N.; Klemmt, S.; Cherotchenko, E.; Betzold, S.; Iff, O.; Nalitov, A. V.; Klaas, M.; Dietrich, C. P.; Kavokin, A. V.; Höfling, S.; Schneider, C. Room-temperature Tamm-plasmon exciton-polaritons with a WSe<sub>2</sub> monolayer. *Nature Communications* **2016**, *7*, 13328, DOI: 10.1038/ncomms13328.
- (8) Flatten, L. C.; He, Z.; Coles, D. M.; Trichet, A. A. P.; Powell, A. W.; Taylor, R. A.; Warner, J. H.; Smith, J. M. Room-temperature exciton-polaritons with two-dimensional WS<sub>2</sub>. *Scientific Reports* **2016**, *6*, 33134, DOI: 10.1038/srep33134.
- (9) Liu, X.; Bao, W.; Li, Q.; Ropp, C.; Wang, Y.; Zhang, X. Control of Coherently Coupled Exciton Polaritons in Monolayer Tungsten Disulphide. *Phys. Rev. Lett.* **2017**, *119*, 027403, DOI: 10.1103/PhysRevLett.119.027403.

- (10) Chen, Y.-J.; Cain, J. D.; Stanev, T. K.; Dravid, V. P.; Stern, N. P. Valley-polarized exciton–polaritons in a monolayer semiconductor. *Nature Photonics* **2017**, *11*, 431–435, DOI: 10.1038/nphoton.2017.86.
- (11) Weisbuch, C.; Nishioka, M.; Ishikawa, A.; Arakawa, Y. Observation of the coupled exciton–photon mode splitting in a semiconductor quantum microcavity. *Phys. Rev. Lett.* **1992**, *69*, 3314–3317, DOI: 10.1103/PhysRevLett.69.3314.
- (12) Gibbs, H. M.; Khitrova, G.; Koch, S. W. Exciton–polariton light–semiconductor coupling effects. *Nature Photonics* **2011**, *5*, 273–273, DOI: 10.1038/nphoton.2011.15.
- (13) Zong, X.; Li, L.; Li, L.; Yu, K.; Liu, Y. Self-hybridized exciton-polaritons in thin films of transition metal dichalcogenides for narrowband perfect absorption. *Opt. Express* **2023**, *31*, 18545–18554, DOI: 10.1364/OE.488392.
- (14) Fei, Z.; Scott, M. E.; Gosztola, D. J.; Foley, J. J.; Yan, J.; Mandrus, D. G.; Wen, H.; Zhou, P.; Zhang, D. W.; Sun, Y.; Guest, J. R.; Gray, S. K.; Bao, W.; Wiederrecht, G. P.; Xu, X. Nano-optical imaging of WSe<sub>2</sub> waveguide modes revealing light-exciton interactions. *Phys. Rev. B* **2016**, *94*, 081402, DOI: 10.1103/PhysRevB.94.081402.
- (15) Hu, F.; Luan, Y.; Scott, M. E.; Yan, J.; Mandrus, D. G.; Xu, X.; Fei, Z. Imaging exciton–polariton transport in MoSe<sub>2</sub> waveguides. *Nature Photonics* **2017**, *11*, 356–360, DOI: 10.1038/nphoton.2017.65.
- (16) Taleb, M.; Davoodi, F.; Diekmann, F. K.; Rosnagel, K.; Talebi, N. Charting the Exciton–Polariton Landscape of WSe<sub>2</sub> Thin Flakes by Cathodoluminescence Spectroscopy. *Advanced Photonics Research* **2022**, *3*, 2100124, DOI: 10.1002/adpr.202100124.
- (17) Kubo, A.; Onda, K.; Petek, H.; Sun, Z.; Jung, Y. S.; Kim, H. K. Femtosecond Imaging of Surface Plasmon Dynamics in a Nanostructured Silver Film. *Nano Letters* **2005**, *5*, 1123–1127, DOI: 10.1021/nl10506655.
- (18) Meyer zu Heringdorf, F.-J.; Chelaru, L.; Möllenbeck, S.; Thien, D.; Horn-von Hoegen, M. Femtosecond photoemission microscopy. *Surface Science* **2007**, *601*, 4700–4705, DOI: 10.1016/j.susc.2007.05.052, Proceedings of the Fifth International Conference on LEEM/PEEM.
- (19) Leißner, T.; Thilsing-Hansen, K.; Lemke, C.; Jauernik, S.; Kjelstrup-Hansen, J.; Bauer, M.; Rubahn, H.-G. Surface Plasmon Polariton Emission Prompted by Organic Nanofibers on Thin Gold Films. *Plasmonics* **2012**, *7*, 253–260, DOI: 10.1007/s11468-011-9301-9.
- (20) Kahl, P.; Wall, S.; Witt, C.; Schneider, C.; Bayer, D.; Fischer, A.; Melchior, P.; Horn-von Hoegen, M.; Aeschlimann, M.; Meyer zu Heringdorf, F.-J. Normal-Incidence Photoemission Electron Microscopy (NI-PEEM) for Imaging Surface Plasmon Polaritons. *Plasmonics* **2014**, *9*, 1401–1407, DOI: 10.1007/s11468-014-9756-6.

- (21) Spektor, G.; Kilbane, D.; Mahro, A. K.; Frank, B.; Ristok, S.; Gal, L.; Kahl, P.; Podbiel, D.; Mathias, S.; Giessen, H.; zu Heringdorf, F.-J. M.; Orenstein, M.; Aeschlimann, M. Revealing the subfemtosecond dynamics of orbital angular momentum in nanoplasmonic vortices. *Science* **2017**, *355*, 1187–1191, DOI: 10.1126/science.aaj1699.
- (22) Joly, A. G.; El-Khoury, P. Z.; Hess, W. P. Spatiotemporal Imaging of Surface Plasmons Using Two-Color Photoemission Electron Microscopy. *The Journal of Physical Chemistry C* **2018**, *122*, 20981–20988, DOI: 10.1021/acs.jpcc.8b05849.
- (23) Dąbrowski, M.; Dai, Y.; Petek, H. Ultrafast Photoemission Electron Microscopy: Imaging Plasmons in Space and Time. *Chemical Reviews* **2020**, *120*, 6247–6287, DOI: 10.1021/acs.chemrev.0c00146.
- (24) Großmann, M.; Black, M.; Jaruschewski, J.; Klick, A.; Leißner, T.; Fiutowski, J.; Rubahn, H.-G.; Bauer, M. Micro-spectroscopy of Buried Short-Range Surface Plasmon Polaritons Supported by Thin Polycrystalline Gold Films. *Plasmonics* **2021**, *16*, 737–746, DOI: 10.1007/s11468-020-01333-1.
- (25) Davis, T. J.; Janoschka, D.; Dreher, P.; Frank, B.; zu Heringdorf, F.-J. M.; Giessen, H. Ultrafast vector imaging of plasmonic skyrmion dynamics with deep subwavelength resolution. *Science* **2020**, *368*, eaba6415, DOI: 10.1126/science.aba6415.
- (26) Kilbane, D.; Prinz, E.; Eul, T.; Hartelt, M.; Mahro, A.-K.; Hensen, M.; Pfeiffer, W.; Aeschlimann, M. Plasmonic wavelength-dependent optical switch. *Opt. Express* **2023**, *31*, 9579–9590, DOI: 10.1364/OE.484035.
- (27) Fitzgerald, J. P. S.; Word, R. C.; Saliba, S. D.; Könenkamp, R. Photonic near-field imaging in multiphoton photoemission electron microscopy. *Phys. Rev. B* **2013**, *87*, 205419, DOI: 10.1103/PhysRevB.87.205419.
- (28) Word, R. C.; Fitzgerald, J. P. S.; Könenkamp, R. Direct coupling of photonic modes and surface plasmon polaritons observed in 2-photon PEEM. *Opt. Express* **2013**, *21*, 30507–30520, DOI: 10.1364/OE.21.030507.
- (29) Fitzgerald, J. P. S.; Word, R. C.; Könenkamp, R. Subwavelength visualization of light in thin film waveguides with photoelectrons. *Phys. Rev. B* **2014**, *89*, 195129, DOI: 10.1103/PhysRevB.89.195129.
- (30) Aeschlimann, M.; Brixner, T.; Differt, D.; Heinzmann, U.; Hensen, M.; Kramer, C.; Lükermann, F.; Melchior, P.; Pfeiffer, W.; Piecuch, M.; Schneider, C.; Stiebig, H.; Strüber, C.; Thielen, P. Perfect absorption in nanotextured thin films via Anderson-localized photon modes. *Nature Photonics* **2015**, *9*, 663–668, DOI: 10.1038/nphoton.2015.159.
- (31) Klick, A.; Wagner, R.; Großmann, M.; Kadem, L. F.; Leißner, T.; Rubahn, H.-G.; Selhuber-Unkel, C.; Bauer, M. Detection and characterization of attenuated multimode waveguiding in SiO<sub>2</sub> slabs using photoemission electron microscopy. *Phys. Rev. B* **2018**, *98*, 085128, DOI: 10.1103/PhysRevB.98.085128.

- (32) Stenmark, T.; Könenkamp, R. Photoemission electron microscopy to characterize slow light in a photonic crystal line defect. *Phys. Rev. B* **2019**, *99*, 205428, DOI: 10.1103/PhysRevB.99.205428.
- (33) Aeschlimann, M.; Brixner, T.; Fenner, F.; Frisch, B.; Folge, P.; Hartelt, M.; Hensen, M.; Loeber, T. H.; Pfeiffer, W.; Pres, S.; Stannowski, B. Direct imaging of photonic band-edge states in golden Vogel spirals using photoemission electron microscopy. *J. Opt. Soc. Am. B* **2023**, *40*, B19–B27, DOI: 10.1364/JOSAB.479667.
- (34) Leißner, T.; Lemke, C.; Fiutowski, J.; Radke, J. W.; Klick, A.; Tavares, L.; Kjelstrup-Hansen, J.; Rubahn, H.-G.; Bauer, M. Morphological Tuning of the Plasmon Dispersion Relation in Dielectric-Loaded Nanofiber Waveguides. *Phys. Rev. Lett.* **2013**, *111*, 046802, DOI: 10.1103/PhysRevLett.111.046802.
- (35) Lemke, C.; Leißner, T.; Klick, A.; Fiutowski, J.; Radke, J. W.; Thomaschewski, M.; Kjelstrup-Hansen, J.; Rubahn, H.-G.; Bauer, M. The complex dispersion relation of surface plasmon polaritons at gold/para-hexaphenylene interfaces. *Applied Physics B* **2014**, *116*, 585–591, DOI: 10.1007/s00340-013-5737-2.
- (36) Hartelt, M.; Terekhin, P. N.; Eul, T.; Mahro, A.-K.; Frisch, B.; Prinz, E.; Rethfeld, B.; Stadtmüller, B.; Aeschlimann, M. Energy and Momentum Distribution of Surface Plasmon-Induced Hot Carriers Isolated via Spatiotemporal Separation. *ACS Nano* **2021**, *15*, 19559–19569, DOI: 10.1021/acsnano.1c06586.
- (37) Kubo, A.; Pontius, N.; Petek, H. Femtosecond Microscopy of Surface Plasmon Polariton Wave Packet Evolution at the Silver/Vacuum Interface. *Nano Letters* **2007**, *7*, 470–475, DOI: 10.1021/nl10627846.
- (38) Lemke, C.; Leißner, T.; Jauernik, S.; Klick, A.; Fiutowski, J.; Kjelstrup-Hansen, J.; Rubahn, H.-G.; Bauer, M. Mapping surface plasmon polariton propagation via counter-propagating light pulses. *Opt. Express* **2012**, *20*, 12877–12884, DOI: 10.1364/OE.20.012877.
- (39) Kahl, P.; Podbiel, D.; Schneider, C.; Makris, A.; Sindermann, S.; Witt, C.; Kilbane, D.; Hoegen, M. H.-v.; Aeschlimann, M.; zu Heringdorf, F. M. Direct Observation of Surface Plasmon Polariton Propagation and Interference by Time-Resolved Imaging in Normal-Incidence Two Photon Photoemission Microscopy. *Plasmonics* **2018**, *13*, 239–246, DOI: 10.1007/s11468-017-0504-6.
- (40) Klick, A.; Großmann, M.; Beewen, M.; Bittorf, P.; Fiutowski, J.; Leißner, T.; Rubahn, H.-G.; Reinhardt, C.; Elmers, H.-J.; Bauer, M. Femtosecond time-resolved photoemission electron microscopy operated at sample illumination from the rear side. *Review of Scientific Instruments* **2019**, *90*, 053704, DOI: 10.1063/1.5088031.
- (41) Cinchetti, M.; Oelsner, A.; Fecher, G. H.; Elmers, H. J.; Schönhense, G. Observation of Cu surface inhomogeneities by multiphoton photoemission spectromicroscopy. *Applied Physics Letters* **2003**, *83*, 1503–1505, DOI: 10.1063/1.1603332.

- (42) Aeschlimann, M.; Bauer, M.; Bayer, D.; Brixner, T.; García de Abajo, F. J.; Pfeiffer, W.; Rohmer, M.; Spindler, C.; Steeb, F. Adaptive subwavelength control of nano-optical fields. *Nature* **2007**, *446*, 301–304, DOI: 10.1038/nature05595.
- (43) Buckanie, N.; Kirschbaum, P.; Sindermann, S.; zu Heringdorf, F.-J. M. Interaction of light and surface plasmon polaritons in Ag Islands studied by nonlinear photoemission microscopy. *Ultramicroscopy* **2013**, *130*, 49–53, DOI: 10.1016/j.ultramic.2013.03.007, Eighth International Workshop on LEEM/PEEM.
- (44) Tidy3D, the full-wave simulator employing the finite-difference time-domain (FDTD) method, developed by Flexcompute Inc. 2024; <https://www.flexcompute.com/tidy3d/solver>.
- (45) Munkhbat, B.; Wróbel, P.; Antosiewicz, T. J.; Shegai, T. O. Optical Constants of Several Multilayer Transition Metal Dichalcogenides Measured by Spectroscopic Ellipsometry in the 300–1700 nm Range: High Index, Anisotropy, and Hyperbolicity. *ACS Photonics* **2022**, *9*, 2398–2407, DOI: 10.1021/acsp Photonics.2c00433.
- (46) Chahshouri, F.; Taleb, M.; Diekmann, F. K.; Rossnagel, K.; Talebi, N. Interaction of excitons with Cherenkov radiation in WSe2 beyond the non-recoil approximation. *Journal of Physics D: Applied Physics* **2022**, *55*, 145101, DOI: 10.1088/1361-6463/ac453a.